Int. J. Heat Mass Transfer. Vol. 23, pp. 483–492.

0017-9310/80/0401-0483 $02.00/0

A NONEQUILIBRIUM HEAT TRANSFER MODEL FOR DISPERSED DROPLET POST-DRYOUT REGIME

PRADIP SAHA
Department of Nuclear Energy, Brookhaven National Laboratory,
Upton, NY 11973, U.S.A.

(*Received* 6 *April* 1979 *and in revised form* 24 *September* 1979)

Abstract – A model for the dispersed droplet post-dryout regime has been developed by considering nonequilibrium heat transfer between the vapor and the liquid droplets. The analysis has resulted in two correlations for the volumetric mass rate of vapor generation. The first correlation is based on the effectiveness of vapor-to-droplet heat transfer, and the second is based on the droplet size. Both the correlations, used with the Heineman correlation for superheated steam, are successful in predicting the wall temperatures in steam–water round tube systems (6–15 mm ID) for a wide range of pressures (29–120 bar), mass fluxes (393–2590 kg/m^2 s), equilibrium qualities (0.17–1.50) and wall superheats (167–556°C).

NOMENCLATURE

A_c, cross-sectional area of the channel [m^2];
A_i, interfacial area density [m^{-1}];
D, tube diameter [m];
G, mixture mass flux [kg m^{-2} s^{-1}];
g, acceleration due to gravity [m s^{-2}];
h, heat transfer coefficient [W m^{-2} °C^{-1}];
i, specific enthalpy [J kg^{-1}];
i_{fg}, latent heat of vaporization [J kg^{-1}];
j, volumetric flux density, $\alpha U_v + (1-\alpha)U_l$ [m s^{-1}];
K_1, effectiveness parameter defined by equation (13);
K, thermal conductivity [W m^{-1} °C^{-1}];
L, distance from the dryout location [m];
L_c, characteristic length [m];
P, pressure [bar] (1 bar = 10^5 N m^{-2});
P_{cr}, critical pressure [bar];
Pr, Prandtl number;
q'', heat flux [W m^{-2}];
Re, Reynolds number;
T, temperature [°C];
T_{sat}, saturation temperature [°C];
U, area averaged velocity [m s^{-1}];
V_{lj}, liquid (droplet) drift velocity, $U_l - j$ [ms^{-1}];
X, actual vapor flow quality;
X_{DO}, dryout quality;
X_e, equilibrium vapor quality;
Z, axial distance along the flow direction [m].

Greek symbols

α, area averaged vapor void fraction;
Γ_v, mass rate of vapor generation per unit volume [kg m^{-3} s^{-1}];
Γ_e, Γ_v under thermal equilibrium assumption [kg m^{-3} s^{-1}];
δ, average droplet diameter at a cross-section [m];
δ_{DO}, average droplet diameter at dryout [m];
μ, dynamic viscosity [kg m^{-1} s^{-1}];
ξ_h, heated perimeter [m];
ρ, density [kg m^{-3}];
σ, surface tension [N m^{-1}].

Subscripts

d, droplet;
DO, dryout;
e, thermal equilibrium condition;
fl, film temperature;
g, saturated vapor;
i, vapor–liquid interface;
l, liquid (saturated in this paper);
v, superheated vapor;
v–d, vapor-to-droplet;
w, wall.

1. INTRODUCTION

AN ACCURATE prediction of wall temperature in the post-dryout (or post-CHF) regime is of great interest for the design of once-through steam generators and for the analysis of a hypothetical loss-of-coolant accident in nuclear reactor systems. Depending on the hydrodynamic and thermal conditions, the flow regime in a post-dryout region can be either a dispersed droplet type or an inverted annular type. In the present paper, only the dispersed droplet flow regime, where the dispersed liquid droplets flow in a continuous vapor medium, will be considered. This type of flow situation occurs downstream of an annular flow when the liquid film at the heated wall disappears because of droplet entrainment and surface evaporation (see Fig. 1).

It is well known that, in general, the assumption of thermal equilibrium in the post-dryout region is not correct [1,2]. Significant amounts of liquid droplets may exist even when the value of the local equilibrium quality exceeds unity. This is due to the fact that heat is not transferred instantaneously from the heated wall to the liquid droplets in the core. On the contrary, most of the heat is first transferred to the vapor next to the

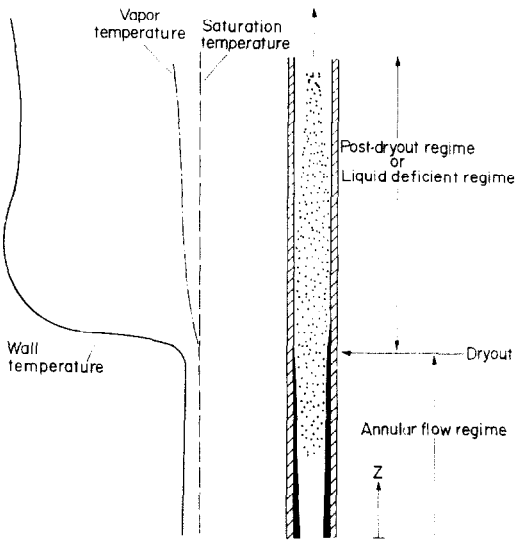

FIG. 1. A typical dispersed-droplet post-dryout regime.

wall, and then a part of that heat is transferred from the vapor to the liquid droplets. As a result, the vapor becomes superheated, and the actual vapor quality becomes less than that calculated under the assumption of thermal equilibrium.

One of the key parameters for a successful prediction of wall temperature is the determination of actual rate of vapor generation. This allows one to calculate the actual vapor quality, which determines the vapor Reynolds number, and the vapor temperature, which is the reference sink temperature for heat transfer from the wall to the vapor. Given the wall heat flux, one can then use a suitable single-phase vapor heat-transfer correlation to calculate the wall temperature. This is the basis of several analytical (semi-empirical) models [1–4] which are reasonably successful in predicting the steady-state post-dryout wall temperature data. To reach the goal, however, the models have to calculate the droplet acceleration, the rate of droplet evaporation, actual vapor quality and the actual vapor temperature by solving four coupled differential equations simultaneously. It is expensive, or at least cumbersome, to incorporate these types of models in a large design or safety code.

In recent years, there has been an increased emphasis on developing a simpler model for the actual vapor quality [5–8]. Unfortunately, none of these simpler models is adequate. For example, the Tong and Young model [5] and the Groeneveld and Delorme model [6] do not predict the correct vapor quality (i.e. the equilibrium quality) at the dryout point. The Plummer *et al.* model [7, 8] and the Tong and Young model [5] assume a linear relationship between the actual vapor quality and the equilibrium vapor quality without offering any justification. Finally, none of the above simplified models is based on mechanistic modeling of the heat-transfer phenomenon involved in the post-dryout regime, and therefore, their applicability to a transient situation like the hypothetical loss-of-coolant accident can be questioned.

The main purpose of the present paper is to remove the shortcomings of the above simplified models. This is done by developing a constitutive equation for the volumetric mass rate of vapor generation from a mechanistic viewpoint. This constitutive equation, along with the conservation of mass and energy, can be used to calculate the local vapor Reynolds number and the local vapor temperature. The constitutive equation has correct boundary conditions and is applicable to any axial heat flux profile.

2. PRESENT MODEL

2.1. *Rate of vapor generation*

As mentioned in the introduction, only the post-dryout regime comprised of spherical dispersed droplets flowing in a continuous vapor medium will be considered here. Several simplifying assumptions have been employed to keep the model tractable. These are:

1. The flow is one-dimensional, i.e. uniform velocity and temperature distribution across a given cross-section of the flow channel. This is valid for the turbulent regime considered in this paper.
2. At any given cross-section, all the droplets are of the same diameter, δ. This droplet diameter can, of course, be a function of time and axial coordinate.
3. The droplets are at saturation temperature. This is justified because the droplets are produced at the pre-dryout region where the assumption of thermal equilibrium holds good.

The droplets can be evaporated by any or all of the following mechanisms:

(a) Direct wall-to-droplet heat transfer, if a droplet can touch the wall.
(b) Radiative heat transfer.
(c) Convective heat transfer between the vapor and the droplets.

It has been shown [9] that for either high wall superheat or high vapor quality, only a few droplets are able to touch or come near the heated wall. This has been found to be true even at moderate wall superheat and moderate vapor quality as reported by Hein [10]. Therefore, in the present paper, the effect of direct wall-to-droplet heat transfer is neglected. The contribution due to the radiative heat transfer has also been found to be negligible within the range of this study. Therefore, the droplets, in the present model, are evaporated only due to the convective heat transfer between the vapor and themselves. In this situation, the mass rate of vapor generation per unit volume, Γ_v, can be expressed by

$$\Gamma_v = \frac{A_i q_i''}{i_{fg}} \tag{1}$$

where A_i is the interfacial area density, q_i'' is the net interfacial heat flux, and i_{fg} is the latent heat of vaporization. For droplet flow regime, the interfacial area density, A_i, can be written as

$$A_i = \frac{6(1-\alpha)}{\delta} \tag{2}$$

where α is the vapor void fraction and δ is the average droplet diameter. The interfacial heat flux, q_i'', may be expressed as

$$q_i'' = h_{v-d}(T_v - T_{sat}) \tag{3}$$

where h_{v-d} is the convective heat-transfer coefficient between the vapor and a droplet, T_v is the vapor temperature, and T_{sat} is the saturation and the droplet temperature. Therefore, equation (1) becomes

$$\Gamma_v = \left[\frac{6(1-\alpha)}{\delta}\right]\left[\frac{h_{v-d}(T_v - T_{sat})}{i_{fg}}\right]. \tag{4}$$

This is the constitutive equation for volumetric mass rate of vapor generation. Notice that the vapor must be superheated, i.e. $T_v > T_{sat}$, to cause droplet evaporation.

2.2. *Prediction of wall temperature*

Since the effects of direct wall-to-droplet and radiative heat transfer are neglected, the wall heat flux may be expressed as

$$q_w'' = h_{w-v}(T_w - T_v) \tag{5}$$

where h_{w-v} is the effective heat-transfer coefficient between the wall and the vapor, and T_v is the local vapor bulk temperature. This approach is quite similar to that taken by the previous researchers [1–8]. The heat-transfer coefficient, h_{w-v}, is usually taken as a function of vapor conductivity, channel hydraulic diameter, vapor Reynolds number and vapor Prandtl number. The vapor temperature, on the other hand, may be calculated by using the conservation of mass and energy, as described below.

For simplicity, let us consider a steady-state, cocurrent flow situation. The vapor continuity and the mixture energy equations (neglecting the effects of kinetic and potential energy) may be written as

$$\frac{dX}{dX_e} = \frac{\Gamma_v}{\Gamma_e} = \frac{\Gamma_v}{(q_w'' \xi_h)/(A_c i_{fg})} \tag{6}$$

and

$$i_v = i_g + \frac{(X_e - X)}{X} i_{fg} \tag{7}$$

where X is the actual vapor quality, X_e is the equilibrium vapor quality, and i_v is the vapor enthalpy. The vapor temperature can then be determined from the caloric equation of state:

$$T_v = T_v(i_v, P). \tag{8}$$

Therefore, it is clear that given the correlations for h_{w-v} and Γ_v, the wall temperature can be determined for a given wall heat flux or vice versa.

3. EFFECTIVE WALL-TO-VAPOR HEAT TRANSFER

It is commonly [2–4, 6] assumed that the effective heat-transfer coefficient between the wall, and the vapor is equal to that for vapor flowing alone at the same velocity as the average vapor velocity in the vapor–droplet mixture. Although at lower vapor qualities, i.e. at higher droplet concentrations, the droplets may augment this heat-transfer coefficient slightly, no attempt is made here to include such changes.

Since the present study is mainly focused to the steam–water systems, the Heineman correlation [11] for superheated steam is used as the effective heat-transfer coefficient between the heated wall and the vapor, i.e.

$$h_{w-v} = 0.0157 \frac{K_{v,fl}}{D} Re_{v,fl}^{0.84} Pr_{v,fl}^{0.33} \left(\frac{L}{D}\right)^{-0.04} \tag{9}$$

for

$$6 < \frac{L}{D} < 60$$

and

$$h_{w-v} = 0.0133 \frac{K_{v,fl}}{D} Re_{v,fl}^{0.84} Pr_{v,fl}^{0.33} \tag{10}$$

for

$$\frac{L}{D} > 60$$

where L is the distance from the dryout location, and the film temperature is the average of the wall and the vapor bulk temperature. The vapor Reynolds number, $Re_{v,fl}$, is expressed as

$$Re_{v,fl} = \frac{\rho_v U_v D}{\mu_{v,fl}} = \frac{GXD}{\alpha \mu_{v,fl}}. \tag{11}$$

4. CORRELATION FOR VAPOR GENERATION RATE

It is seen from equation (4) that the calculation of volumetric mass rate of vapor generation requires knowledge of the vapor void fraction, α, the vapor-to-droplet heat-transfer coefficient, h_{v-d}, and the droplet diameter, δ. Out of these three, the droplet diameter is probably the most difficult one to determine. To circumvent the problem, the present study is divided in two parts. In the first part, equation (4) is rewritten as

$$\Gamma_v = K_1 \frac{K_v(1-\alpha)(T_v - T_{sat})}{D^2 i_{fg}} \tag{12}$$

where

$$K_1 \equiv 6\left(\frac{h_{v-d}\delta}{K_v}\right)\left(\frac{D}{\delta}\right)^2. \tag{13}$$

The nondimensional parameter K_1 may be viewed as a measure of the effectiveness of vapor-to-droplet heat transfer, and is correlated in terms of local flow variables such as pressure, mass flux, vapor quality,

vapor void fraction, etc., but excluding the droplet diameter.

In the second part, the droplet diameter, δ, is correlated based on a suitable vapor-to-droplet heat-transfer coefficient and the information obtained from the first part, i.e. K_1 correlation. Both the parts, however, require a correlation for vapor void fraction which is described below.

4.1. *Vapor void fraction in dispersed droplet flow*

Following the drift-flux model [12], an expression for vapor void fraction is obtained in terms of actual vapor quality, phase densities, mixture mass-flux, droplet distribution parameter and the droplet drift velocity. The droplet distribution parameter is taken as unity for the turbulent flow being considered in this study, and has been found to be valid in [13, 14]. Therefore, the expression becomes

$$(1-\alpha)=\frac{1-X}{\left[1+\dfrac{X(\rho_l-\rho_v)}{\rho_v}\right]+\dfrac{\rho_l V_{lj}}{G}}. \tag{14}$$

The droplet drift velocity, V_{lj}, for vertical upflow and high void fractions encountered in the dispersed droplet regime, may be taken as

$$V_{lj}=-\alpha(U_v-U_l)\approx -1.41\left[\frac{g\sigma(\rho_l-\rho_v)}{\rho_v^2}\right]^{0.25} \tag{15}$$

which is similar to that suggested in [15].

4.2. *Part 1:* K_1 *correlation*

The thermal equilibrium condition in the pre-dryout region implies:

$$\text{at } Z=Z_{DO},\quad X=X_e=X_{DO} \quad \text{and} \quad T_v=T_{sat}. \tag{16}$$

In view of equation (12), this condition also implies that the vapor generation rate, Γ_v, at the start of the post-dryout region is zero. Given a value for K_1, one can now solve equations (5)–(8), (9) or (10), (12) and (14) simultaneously to calculate the wall temperature for a given wall heat flux.

Considering several aspects of the dispersed droplet flow, it is postulated that the value of K_1 should increase with the distance from the dryout location (because of increasing vapor turbulence level and decreasing droplet size), and should increase with decreasing pressure (because of increasing relative velocity). Based on the round tube, steam–water, high wall temperature data ($T_w - T_{sat} > 222°C$) of [2, 16], the effectiveness parameter K_1 is then correlated by

$$K_1=6300\left(1-\frac{P}{P_{cr}}\right)^2\left[\left(\frac{GX}{\alpha}\right)^2\frac{D}{\rho_v\sigma}\right]^{0.5}. \tag{17}$$

The high wall temperature data were selected so that the effect of direct wall-to-droplet heat transfer remained negligible. The range of data used to develop the correlation includes: two tube diameters (12.6 and 14.9 mm ID), and a wide range of pressures (29–120 bar), mass-fluxes (393–2591 kg/m^2 s), wall heat fluxes (45–127 W/cm^2) and equilibrium qualities (0.18–1.50). The RMS error of the correlation for the prediction of wall temperature is 4.82% for 895 data points of [2, 16].

An estimate of the droplet diameter is obtained from correlation (17), definition (13) and the following heat-transfer coefficient [18] between the vapor and the droplet:

$$h_{v-d}=\frac{K_v}{\delta}\left[2+0.459\left\{\frac{\rho_v(U_v-U_l)\delta}{\mu_v}\right\}^{0.55}Pr_v^{0.33}\right]. \tag{18}$$

Sample calculations yield droplet diameters in the range of 100–600 μm. The corresponding values for the droplet Weber number, $\rho_v(U_v-U_l)^2\delta/\sigma$, range from 0.1 to 1. These values are much smaller than the critical Weber number values (6.5 and greater) usually assumed as the droplet breakup criterion [1–3].

4.3. *Part 2: Correlation for droplet diameter*

Based on the expected range of droplet Weber number, found in Part 1, it is assumed that there is no droplet breakup downstream of the dryout location. For steady-state, this implies:

$$\frac{\delta}{\delta_{DO}}=\left[\frac{1-X}{1-X_{DO}}\right]^{1.3}. \tag{19}$$

The task is now reduced to finding a correlation for the average droplet diameter at dryout, δ_{DO}.

Optimum values of the droplet diameter at dryout location, δ_{DO}, are found from selected high wall temperature runs of [2, 16] by using equations (19), (18), (14), (9) or (10), and (4)–(8), simultaneously. These values ranged from 115–700 μm and are tabulated in [17]. Higher the mass-flux, lower is the droplet size. Also, the droplet size decreases with the decrease in system pressure. A mechanistic correlation, described below, has been developed from these optimum values.

Let us consider the pre-dryout annular flow region where the droplets are entrained from the wavy liquid film at the wall to the vapor core. The most common type of entrainment mechanism is the shearing off the tops of the large amplitude roll waves from the wave crests by the turbulent gas or vapor flow [19]. The size of the droplets thus produced can be expected to be proportional to the roughness height seen by the vapor flow. It is known that this roughness height increases with increasing film thickness [20]. Therefore, the droplet size can be expected to be proportional to the film thickness.

Ishii and Grolmes [19] have shown that for the turbulent regime the volumetric vapor flux density, j_g, (or the vapor quality for a given mass flux) at the inception of droplet entrainment depends only on the liquid and vapor properties, and not on the tube diameter. As the void fraction relationship is not a strong function of the tube diameter, the vapor void

fraction at which droplet entrainment starts is not expected to be a strong function of tube diameter. However, for a particular value of void fraction in a pure annular flow with no entrainment, the film thickness is *proportional* to the tube diameter and is given by $D(1-\sqrt{\alpha})/2$. This implies that the film thickness at the inception of droplet entrainment may be expected to be proportional to the tube diameter. Since the film thickness at dryout is zero, it follows that the average film thickness over which droplet entrainment occurs may also be expected to be proportional to the tube diameter. Therefore, the average droplet diameter at dryout is assumed to be proportional to the tube diameter.

It is also known that the deformation of the wave crests is governed by a balance between inertia and surface tension forces, as defined by the Weber number $\rho_g(U_g - U_{fl})^2 L_c/\sigma$. Because the average liquid film velocity, U_{fl}, is small compared to the average vapor velocity, U_g, and the vapor void fraction is high in the annular flow regime, the relative velocity term in the Weber number may be replaced by the volumetric vapor flux density, j_g, or αU_g. The length parameter, $\{\sigma/[g(\rho_l - \rho_v)]\}^{1/2}$, which has been used successfully by Ishii and Grolmes [19] in their inception criteria for droplet entrainment, is chosen as the characteristic length.

Based on the above arguments and the optimum values of δ_{DO} mentioned earlier, the following correlation is obtained:

$$\frac{\delta_{DO}}{D} = 1.47\left[\frac{\rho_g j_{g,DO}^2\{\sigma/[g(\rho_l - \rho_g)]\}^{1/2}}{\sigma}\right]^{-0.675} \tag{20}$$

where $j_{g,DO}$ is the volumetric vapor flux density at dryout, i.e. GX_{DO}/ρ_g. This equation along with the assumption of no droplet breakup yields for steady-state:

$$\frac{\delta}{D} = 1.47\left[\frac{\rho_g j_{g,DO}^2\{\sigma/[g(\rho_l - \rho_g)]\}^{1/2}}{\sigma}\right]^{-0.675} \times \left(\frac{1-X}{1-X_{DO}}\right)^{1/3}. \tag{21}$$

The above equation can now be used to calculate the actual rate of vapor generation in accordance with equation (4). The Heineman correlation (9) or (10) is then used to predict the wall temperatures for steam–water systems. The RMS error for this δ_{DO}-correlation is 5.34% for the same 895 data points of [2] and [16].

5. RESULTS AND DISCUSSION

As a result of the boundary condition (16), equation (6) becomes:

$$\left.\frac{dX}{dX_e}\right|_{X_e = X_{DO}} = 0 \tag{22}$$

i.e. the actual vapor quality distribution starts with a zero slope.

At a point downstream of the dryout location, however, the value of the equilibrium vapor quality increases, and according to equation (7), the vapor becomes superheated. This causes further vapor generation in accordance with equation (4) or (12) and the actual vapor quality distribution starts to grow. As the actual vapor quality approaches unity, the vapor void fraction also approaches unity and, therefore, equation (4) or (12) dictates that the rate of vapor generation or the slope of the actual quality distribution approaches zero once again. This feature of the present model is shown in Fig. 2(a) where Run No. 5337 of [2] has been taken as the test case. Notice that the model starts from the dryout location and, therefore, does not have to be matched artificially at the dryout location like the Groeneveld and Delorme model [6]. Also note that the actual vapor quality does not have to increase linearly with the equilibrium quality, as assumed in the Plummer *et al.* [7,8] and the Tong and Young [5] models.

Two limiting models are also shown in Fig. 2(a). The "no further evaporation" model or the "frozen droplet" model assumes that there is no heat transfer between the superheated vapor and the droplets, and therefore, the actual vapor quality remains at the value of the dryout quality. Consequently, all the heat added to the system is utilized in raising the vapor temperature. The results corresponding to this model may be obtained by substituting $K_1 = 0$ in equation (12) or $\delta \to \infty$ in equation (4).

The "thermal equilibrium" model is the other extreme. This model assumes that the heat-transfer process between the vapor and the droplets is so efficient that the vapor *does not* become superheated until the value of the equilibrium vapor quality exceeds unity. Therefore, accordintg to the thermal equilibrium model:

$$X = X_e \quad \text{and} \quad i_v = i_g \quad \text{for } X_e \leqslant 1 \tag{23a}$$

and

$$X = 1 \quad \text{and} \quad i_v = i_g + (X_e - 1)i_{fg} \quad \text{for } X_e \geqslant 1. \tag{23b}$$

This model may also be realized by substituting $K_1 \to \infty$ in equation (12) or $\delta \to 0$ in equation (4).

The predictions for vapor superheat corresponding to various models are shown in Fig. 2(b). It can be seen that according to the present model, significant vapor superheat is possible even if the equilibrium vapor quality is less than unity. In Fig. 2(c), the values for the droplet diameter δ and the effectiveness parameter K_1 are shown for both of the present correlations. An inspection of Figs. 2(a), 2(b), and 2(c) reveals that a large difference in the droplet diameter ($\sim 50\ \mu$m) or the effectiveness parameter K_1 ($\sim 25\%$) produces a rather small difference in the actual vapor quality ($\sim 2\%$) and the vapor superheat (~ 20°C). That is to say that the actual vapor quality and the vapor superheat, which are the critical items for the prediction of wall temperature, are not very sensitive to

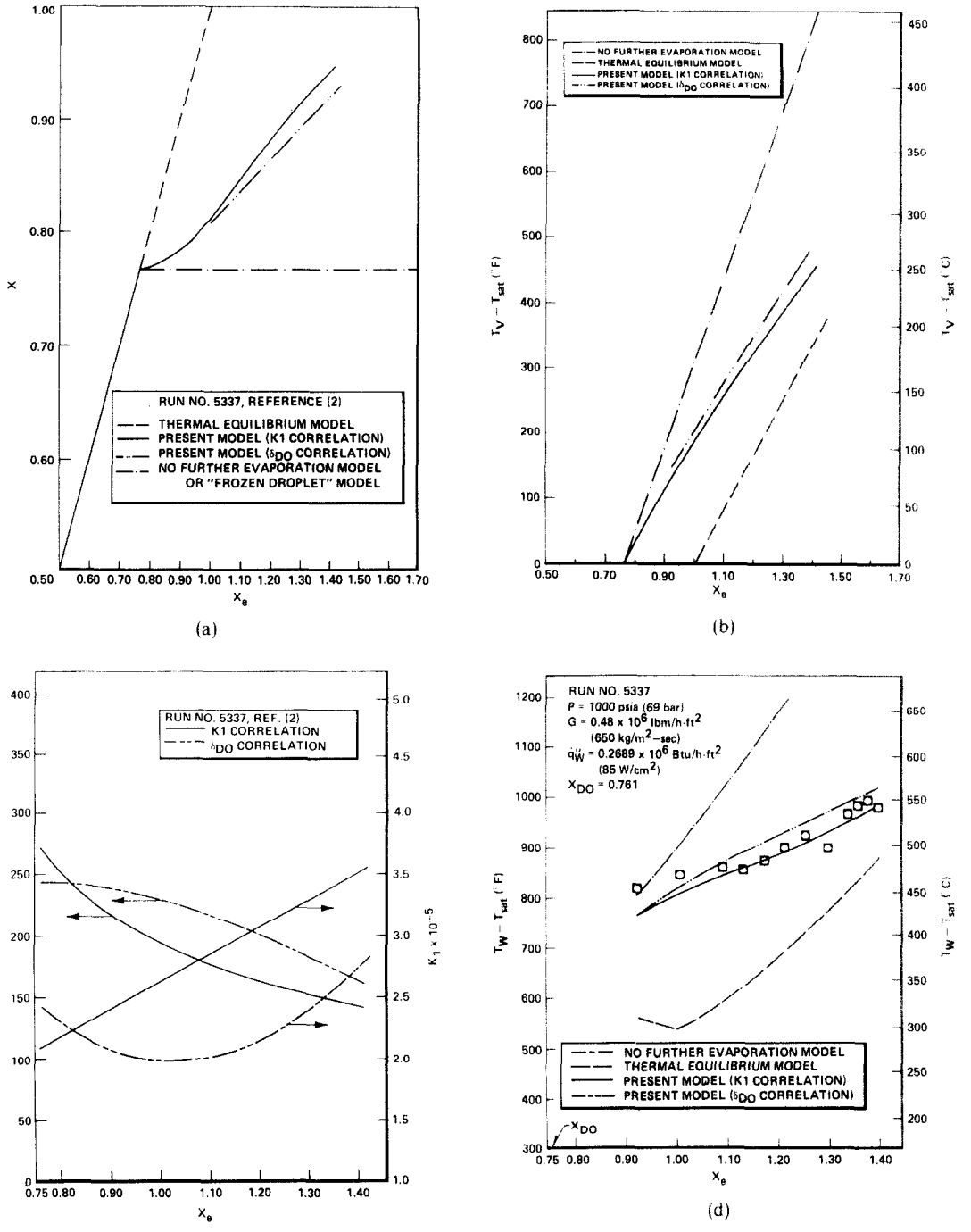

FIG. 2(a). Actual vapor quality for various models. (b) Vapor superheat for various models (Run No. 5337 [2]). (c) Droplet diameter and effectiveness parameter for present correlations. (d) Comparison of various models with wall superheat data of Bennett *et al.* [2].

the values of the droplet diameter or the effectiveness parameter. The predictions for wall superheat, i.e. $T_w - T_{sat}$, for the same run are shown in Fig. 2(d). It can be seen that the experimental data fall between the two limiting models, and the data are well predicted by the present correlations.

Similar comparisons of the wall superheat data of [2] at various mass fluxes, but at the same pressure (P = 69 bar), are shown in Fig. 3. In Fig. 4, the wall superheat data of [16] at various pressures but at the same mass fluxes are compared with the present model. In general, the agreement between the data and the present correlations is good.

The present correlations, in general, tend to over-

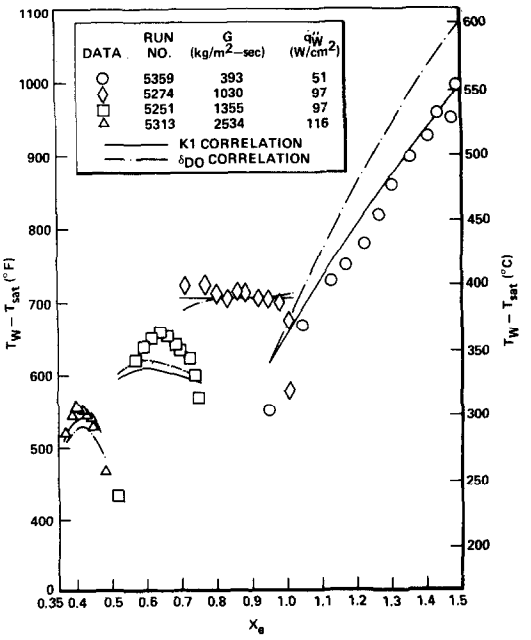

FIG. 3. Comparison of present correlations with wall superheat data of Bennett *et al.* [2], at 69 bar.

predict the wall temperature just downstream of the dryout location. This is to be expected since the model does not take into account the effects of axial heat conduction, rivulets and droplet deposition. Some or all of these items can be important near the dryout location.

The predicted wall temperatures have been compared also with the data of Janssen and Kervinen [21],

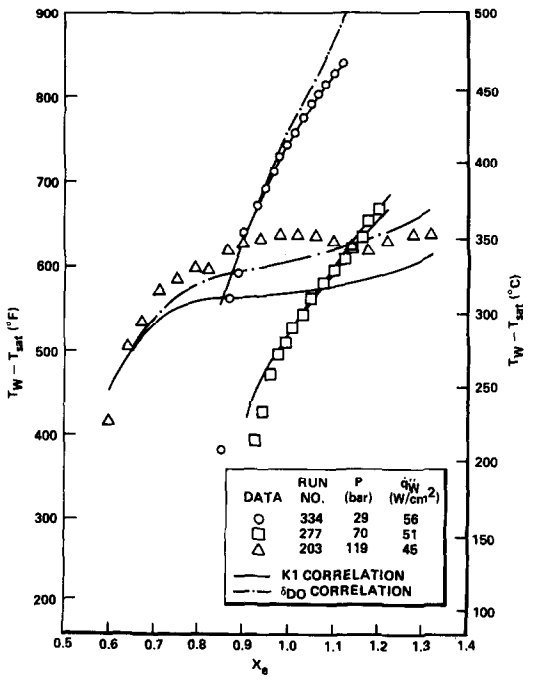

FIG. 4. Comparison of present correlations with wall superheat data of Ling *et al.* [16], at 500 kg/m² s.

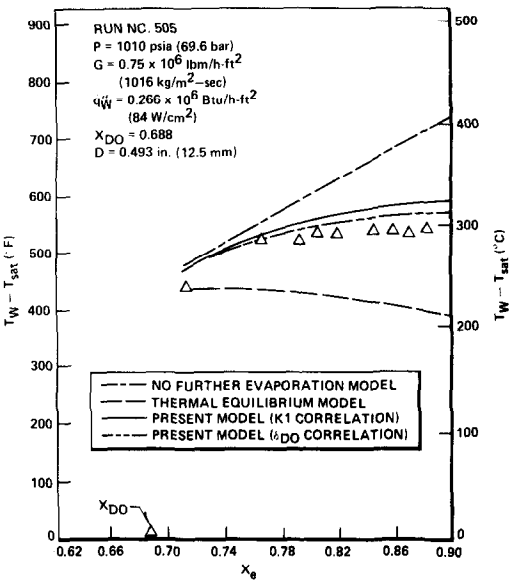

FIG. 5. Comparison of various models with wall superheat data of Janssen and Kervinen [21].

Era *et al.* [22], and the low wall temperature data of Bennett *et al.* [2] and Ling *et al.* [16]. These data *were not* used to develop the correlations. Satisfactory agreement between the data and the predicted wall temperatures has been found (Figs. 5 and 6 serve as examples). Finally, the predictions are compared with the data of Keeys *et al.* [23], which were taken in a tube with a chopped cosine axial heat flux distribution. Once again, good agreement between these data and the present prediction is found (see Fig. 7 for example). This provides one with confidence that the correlations presented here can be used in nonuniform axial heat flux situations.

From the results presented above, it is apparent that either the K_1-correlation or the δ_{DO}-correlation may be used for the prediction of wall temperature in post-dryout dispersed droplet flow regime. Although the correlations have been developed from steam–water data, the mechanistic nature of the model suggests their possible application to other fluid systems as well.

The effect of radiative heat transfer has been neglected in the present study. Calculation showed that the effect of radiative heat transfer was small compared to that of the convective heat transfer for the data examined here, even in the worst combination of the lowest mass flux and the highest wall temperature. However, the effect of radiation would be important for a situation with lower mass flux or higher wall temperature than the worst case of the present study, and should be included.

It is fair to mention that two other independent studies [24, 25] on the same topic were carried out almost at the same time. The model of Jones and Zuber [24] starts from the same basic equations as those of the present model. However, they subtracted the actual vapor continuity equation from the equilibrium equation and wrote the resulting expression as a first

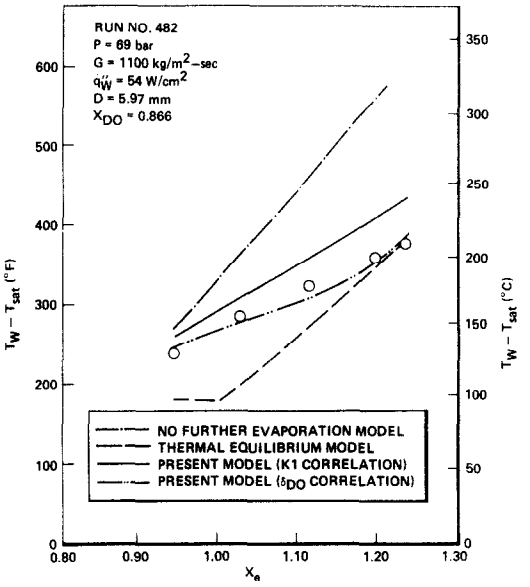

FIG. 6. Comparison of various models with wall superheat data of Era *et al.* [22].

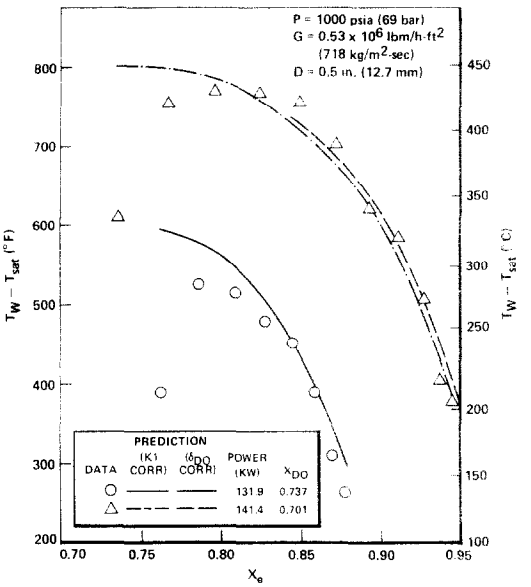

FIG. 7. Comparison of present correlations with wall superheat data of Keeys *et al.* [23].

order relaxation equation with $(X_e - X)$ as the dependent variable and the superheat relaxation number, N_{sr}, as a parameter. A correlation for the superheat relaxation number was then developed from the nitrogen data of Forslund and Rohsenow [26] and the steam–water data of Bennett *et al.* [2].

The model of Chen *et al.* [25], on the other hand, uses the analogy between the heat and momentum transfer to predict the convective heat flux from the wall to the vapor. A local correlation for actual quality, neglecting the history effects of droplet evaporation, is developed based on the steam–water round tube data. This correlation is used to calculate the vapor temperature and the vapor Reynolds number which is needed to compute the two-phase friction factor. The reference [25] shows good agreement between the calculated and the "inferred" experimental values of the actual quality, but does not show any comparison between the predicted and the experimental values of the wall temperatures.

A detailed comparative study of the present and the above two models is beyond the scope of this paper. A

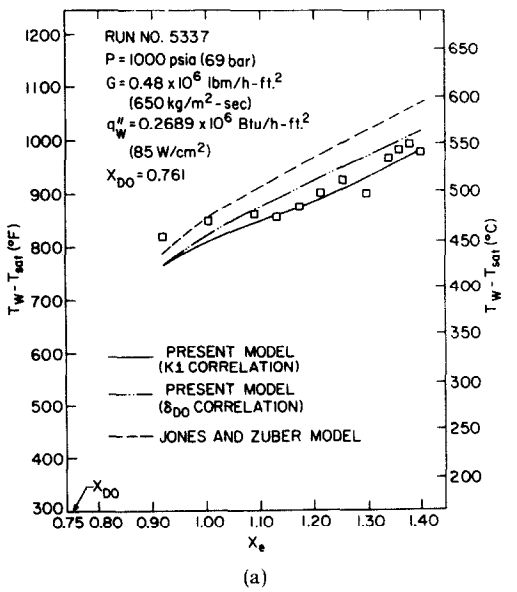

(a)

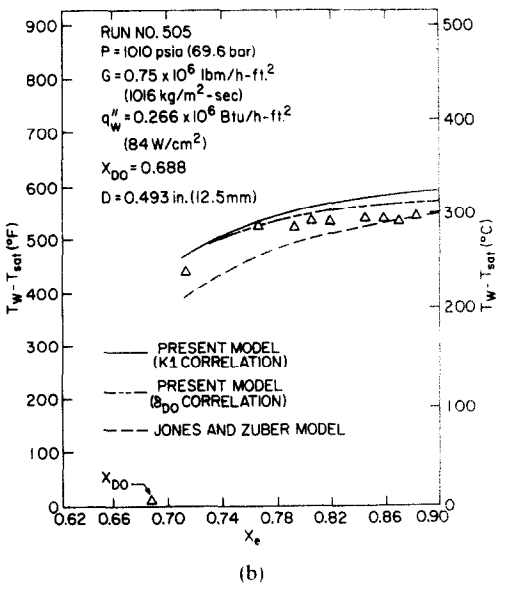

(b)

FIG. 8(a). Comparison between the present model and the model of Jones and Zuber with data of Bennett *et al.* [2]. (b) Comparison between the present model and the model of Jones and Zuber with data of Jannssen and Kervinen [21].

separate endeavor is recommended for that purpose. However, to provide the reader with a comparative feeling, two comparisons between the predictions of the present model and those of the Jones and Zuber model are shown in Figs. 8(a) and 8(b). It is seen that the predictions are of comparable accuracy.

6. SUMMARY AND CONCLUSIONS

A constitutive equation for the volumetric mass rate of vapor generation in dispersed droplet post-dryout regime has been developed. Based on the high wall temperature steam–water round tube data, two correlations for this rate of vapor generation have been developed.

The first correlation, i.e. the K_1-correlation, does not involve explicit calculation of droplet diameter. Rather, it is based on the effectiveness of vapor-to-droplet heat transfer and is expressed as a function of local flow variables like pressure, mass-flux, quality, void fraction, and tube diameter.

The second correlation, i.e. the δ_{DO}-correlation, on the other hand, provides one with a calculational method for droplet diameter, and thus a more complete physical description of the flow.

Both the correlations, used with the Heineman correlation for superheated steam, are successful in predicting the wall temperature data in round tube, steam–water systems from a wide range of pressures, mass fluxes, wall temperatures and vapor qualities. The correlations can be used in nonuniform axial heat flux situation, and because of their mechanistic nature, they can also be applied to transient situations with some degree of confidence.

Acknowledgements – Most of the work was supported by and carried out at Nuclear Energy Division of General Electric Company. The author thanks Drs. B. S. Shiralkar and G. E. Dix for their comments and suggestions. Assistance rendered by Brookhaven National Laboratory for the preparation of the manuscript and Dr. O. C. Jones, Jr. for Figs. 8(a) and 8(b) are highly appreciated.

REFERENCES

1. R. P. Forslund and W. M. Rohsenow, Dispersed flow film boiling, *J. Heat Transfer* **90C**, 399–407 (1968).
2. A. W. Bennett, G. F. Hewitt, H. A. Kearsey and R. K. F. Keeys, Heat transfer to steam–water mixtures flowing in uniformly heated tubes in which the critical heat flux has been exceeded, UKAEA Research Group Report AERE-R5373 (1967).
3. D. C. Groeneveld, The thermal behavior of a heated surface at and beyond dryout, AECL-4309 (1972).
4. V. I. Subbotin, O. V. Remizov and V. A. Vorobev, Calculation of the temperature profile of the wall in the region of deteriorating heat transfer, *Teplofiz. Vysok. Temper.* **12** (4), 785–789 (1974).
5. L. S. Tong and J. D. Young, A phenomenological transition and film boiling heat transfer correlation, *Heat Transfer 1974, Proceedings of the 5th Int. Heat Transfer Conference*, Vol. IV, pp. 120–124. JSME and SCEJ, Tokyo (1974).
6. D. C. Groeneveld and G. G. Delorme, Prediction of thermal nonequilibrium in the post-dryout regime, *Nucl. Engng Design* **36**, 17–26 (1976).
7. D. N. Plummer, Post-critical heat transfer to flowing liquid in a vertical tube, Ph.D. Thesis, Dept. of Mech. Eng., Massachusetts Institute of Technology, Cambridge, MA (1974).
8. D. N. Plummer, P. Griffith and W. M. Rohsenow, Post-critical heat transfer to flowing liquid in a vertical tube, Paper No. 76-CSME/CSChE-13, Presented at the 16th National Heat Transfer Conf., St. Louis (1976).
9. O. C. Iloeje, D. N. Plummer, W. M. Rohsenow and P. Griffith, A study of wall rewet and heat transfer in dispersed vertical flow, M.I.T. Report 72718-92 (1974).
10. R. A. Hein, Investigation of the flow boiling curve for high pressure water, MSME Project Report, Dept. of Mechanical Engineering, University of California, Berkeley (1976).
11. J. B. Heineman, An experimental investigation of heat transfer to superheated steam in round and rectangular tubes, ANL-6213 (1960).
12. N. Zuber and J. A. Findlay, Average volumetric concentration in two-phase flow systems, *J. Heat Transfer* **87C**, 453–468 (1965).
13. M. Cumo, G. Ferrari and G. E. Farello, A photographic study of two-phase highly dispersed flows, Paper presented at European Two-Phase Flow Group Meeting, Milan (1970).
14. M. Cumo, G. E. Farello, G. Ferrari and G. Palazzi, On two-phase highly dispersed flows, *J. Heat Transfer* **96C**, 496–503 (1974).
15. M. Ishii, One-dimensional drift-flux model and constitutive equations for relative motion between phases in various two-phase flow regimes, ANL-77-47 (1977).
16. C. H. Ling, K. M. Becker, S. Hedberg and G. Strand, Temperature distribution for the post-burnout regime in a round tube, Royal Institute of Technology, Laboratory of Nuclear Engineering, KTH-NEL-16, Stockholm (1971).
17. P. Saha, B. S. Shiralkar and G. E. Dix, A post-dryout heat transfer model based on actual vapor generation rate in dispersed droplet regime, ASME Paper 77-HT-80, presented at the 17th National Heat Transfer Conference, Salt Lake City (1977).
18. S. L. Soo, *Fluid Dynamics of Multiphase System*, p. 23. Blaisdell, Waltham, MA (1967).
19. M. Ishii and M. A. Grolmes, Inception criteria for droplet entrainment in two-phase concurrent film flow, *A.I.Ch.E. Jl* **21**(2), 308–318 (1975).
20. G. F. Hewitt and N. S. Hall-Taylor, *Annular Two-Phase Flow*, pp. 87–93. Pergamon Press, Oxford (1970).
21. E. Janssen and J. A. Kervinen, Film boiling and rewetting, General Electric Co. Report NEDO-20975 (1975).
22. A. Era, G. P. Gaspari, A. Hassid, A. Milani and R. Zavattarelli, Heat transfer data in the liquid deficient region for steam–water mixtures at 70 kg/cm^2 flowing in tubular and annular conduits, CISE-R-184, Topical Report 11 (1966).
23. R. K. F. Keeys, J. C. Ralph and D. N. Roberts, Post-burnout heat transfer in high pressure steam–water mixtures in a tube with cosine heat flux distribution, UKAEA Research Group Report AERE-R 6411 (1971).
24. O. C. Jones, Jr. and N. Zuber, Post-CHF heat transfer: a nonequilibrium relaxation model, ASME paper 77-HT-79, Paper presented at the 17th National Heat Transfer Conference, Salt Lake City (1977).
25. J. C. Chen, F. T. Ozkaynak and R. K. Sundaram, Vapor heat transfer in post-CHF region including the effect of thermodynamic nonequilibrium, *Nucl. Engng Design* **51**, 143–155 (1979).
26. R. P. Forslund and W. M. Rohsenow, Thermal nonequilibrium in dispersed flow film boiling in a vertical tube, MIT Report 75312-44 (1966).

UN MODELE DE DESEQUILIBRE THERMIQUE POUR DES GOUTTELETTES DISPERSEES APRES ASSECHEMENT

Résumé — On développe un modèle de régime de gouttelettes dispersées après l'assèchement, en considérant un déséquilibre thermique entre la vapeur et les gouttelettes liquides. L'analyse conduit à deux formulations pour le débit massique de la vapeur formée. La première formulation est basée sur l'efficacité du transfert thermique entre la vapeur et les gouttes, et la seconde sur la dimension des gouttes. Les deux expressions, jointes à la formule de Heineman pour la vapeur surchauffée, prédisent correctement les températures de la paroi de tubes circulaires (diamètre intérieur de 6 à 15 mm) pour un large domaine de pression (29 à 120 bar), de débit massique (393 à 2590 kg/m^2 · s), de qualité d'équilibre (0,17 à 1,50) et de surchauffe de paroi (167 à 556°C).

EIN NICHTGLEICHGEWICHTS-WÄRMEÜBERTRAGUNGSMODELL FÜR DIE TROPFENSTRÖMUNG IM BEREICH DER SIEDEKRISE 2. ART

Zusammenfassung—Auf der Basis der Nichtgleichgewichts-Wärmeübertragung zwischen Dampf- und Flüssigkeitstropfen wurde ein Modell für die Tropfenströmung im Bereich der Siedekrise 2. Art entwickelt. Als Ergebnis wurden zwei Korrelationen für die volumetrische Verdampfungsgeschwindigkeit erhalten. Die erste Korrelation basiert auf der Güte des Wärmeübergangs vom Dampf an die Tropfen, der zweite auf der Tropfengröße. Mit der Heinemann-Korrelation für überhitzten Dampf erweisen sich beide Korrelationen als geeignet zur Bestimmung der Wandtemperatur von wasser- und dampfdurchströmten runden Rohren in einem weiten Parameterbereich. Die Parameterbereiche sind: Rohrdurchmesser (6–15 mm), Druck (21–120 bar), Massenstromdichte (393–2590 kg/m^{2}s), Dampfmassengehalt (0,17–1,50), Wandüberhitzung (167–556°C).

НЕРАВНОВЕСНАЯ МОДЕЛЬ ТЕПЛООБМЕНА В ДИСПЕРСНО-КАПЕЛЬНОМ ЗАКРИТИЧЕСКОМ РЕЖИМЕ

Аннотация Разработана модель дисперсно-капельного закритического режима неравновесного переноса тепла между паром и каплями жидкости. В результате анализа получено два соотношения для скорости объёмной массопередачи при парообразовании. В основу первого соотношения положена эффективность переноса тепла от пара к капле, а второго — размер капель. Оба соотношения совместно с соотношением Хайнемана для перегретого водяного пара могут успешно использоваться для расчета температуры стенки круглых трубчатых паро-водяных систем (с внутренним диаметром от 6 до 15 мм) в широком диапазоне давлений (29–120 бар), массовых потоков (393–2590 кг/м^2 · сек) и перегревов стенки (167–556°C).